Romanian Journal of Mechanics
Volume 4, Issue 1/2019, pp 3-14, ISSN 2537 - 5229, *rjm.journals.srmta.ro*

NUMERICAL AND EXPERIMENTAL INVESTIGATIONS OF THE BEHAVIOUR OF A FRAME EQUIPPED WITH NITI WIRES. PART 1. THE CASE OF ABSENCE OF NITI WIRES

Cristian RUGINĂ [*], Ciprian DRAGNE [*], Iulian GIRIP, Daniel BALDOVIN [*], Luciana MAJERCSIK [**]

[*] Institute of Solid Mechanics, Romanian Academy, Bucharest
[**] Transilvania University of Brasov

Corresponding author: Cristian RUGINĂ, E-mail: rugina.cristian@imsar.ro

Abstract Numerical and experimental analysis on the vibrations of a 2 level frame structure equipped/or not with shape memory alloy wires is presented in this study. The first part of the study, the present article treats the frame in the absence of NITi wires, while the second part considers the structure equiped with NiTi wires. The structural model consists of 2 level structure with constant height of 350 mm and the width of each plate 300 mm. The plates are made out of plexiglass plates to create a rigid plan system and the columns are circular hollow brass rods of diameter 4.00 mm and thickness of 0.40 mm. Vibration system tests are performed in order to investigate the behavior of the frame equipped or not with NiTi wires and the effect on the SMA wires on the amplitudes reduction, the transformation behavior for wires and avoiding of the resonance states. The FEM simulations determines the fields of displacement and normal modes. The results are validated with experimental results.

Key words: Shape-memory alloys, experimental data, seismic protection devices, earthquake engineering.

1. INTRODUCTION

The shape memory alloys (SMA) have the property of changing the shape, the natural frequency and the mechanical properties of a structure by providing a source such as temperature, stress, electrical field or magnetic field [1-3]. The SMA can be used as actuators, sensors to control the dynamical behavior of a structure by embedding them into the structure [4, 5]. The SMA has two remarkable properties namely: shape memory effect and superelasticity [6-9]. When the structure is mechanically loaded below the martensite finish temperature, it regains its original shape after removing the loading by heating the structure above the austenite finish temperature. This phenomenon is known as the shape memory effect. The superelasticity is the reversible response to the load caused by phase transformation.

In the 1960s were developed some nickel-titanium alloys with a composition of 53-57% nickel by weight, that exhibited an unusual effect: the deformed specimens with residual strains of 6-10% regained their original shape after a thermal cycle. This effect became as the shape-memory effect. Shape memory alloys (SMA) are materials capable of very large recoverable inelastic strain (of the order of 10%) [10]. Numerous works have been done in the area of using NiTi for vibration and mechanical characterization with and without embedding into different types of composites [11-14]. Researchers have been used different diameters of SMA wire, composition, different environment condition etc. However, there is scope for investigation on improvisation of SMA properties with structure by experimental, numerical and/or analytical techniques.

It is known the application of the shape memory alloy in earthquake engineering as both vibration control and isolation elements for buildings and bridges [15, 16]. The Basilica of St. Francis in Assisi, Italy damaged during the 1999 earthquake was restored maintaining the original concept of the structure by connecting the tympanum and the roof by superelastic SMA rods. The SMA rods have the role of reducing the seismic forces transferred to the tympanum [17, 18].

The old (XIV century) bell tower of the church of San Giorgio in Trignano, Italy made of masonry was seriously damaged during the 1996 earthquake. The rehabilitation of the bell tower consisted in the insertion of four vertical prestressing steel tie bars in the internal corners of the structure with the aim of increasing its flexural strength. The tie bars were formed by six tight-screwing segments placed in series with four SMA devices made of several superelastic wires. The main goal of the restoration was to guarantee constant compression on the masonry by post-tensioning the SMA devices [19, 20].

Fugazza [4, 21] tested a number of superelastic NiTi wires and bars of different size (diameter of 0.76, 1 and 8 mm). He focused on the cyclic behavior of such elements and performed both static and dynamic tests at loading frequencies of 0.001 and 1 Hz respectively. The maximum deformation attained during the experiments was 6%, reached by subsequent increments of 1%. The SMA performances in control vibrations and earthquake engineering, such as damping properties, material strength and reentering capability are discussed in [22-25].

The source of the mechanical behavior of SMAs is a crystalline phase transformation between the austenite and martensite. Martensitic structure is obtained from austenite with application of mechanical load or decrease in temperature. Upon heating or reduction of stress, the austenitic structure is recovered.

The temperature at which the alloy remembers its high temperature form when heated can be adjusted by slight changes in alloy composition and through heat treatment. In the NiTi, for instance, it can be changed from above +100 $^{\circ}$C to below -100 $^{\circ}$C.

The main object of this study is the experimental investigation of the vibration system tests of a 2 level frame structure equipped with shape memory alloy wires. The first part of this study, the present paper, treats the case of absence of NiTi wires, while a future paper will consider the structure equiped with NiTi wires. Comparisons with numerical FEM results will be provided.

2. EXPERIMENTAL SETUP AND MEASUREMENTS

The experimental setup (fig.1) consists of a 2-level frame structure, the vibration system, and a data acquisition system measuring the displacements of the structure at different vibration frequencies, for two configurations of sensor positions (Fig.2, Fig.3).

The structure consists (Fig.1, Fig.2, Fig.3) of 2 level frames made of plexiglass supported by hollow brass rods and an additional plexiglass level (level 0) that attach the structure to the vibration system, providing also the stability for the supporting rods. The plexiglass plates were positioned at level of 350mm high one from another. Additional steel plates were attached with screws to the plexiglass plates to give a more realistic approach of weight of real existing structures. The steel plates have been manufactured to weight 0.5 kg each, with geometric dimensions of 160mm×80mm×6.2mm. The geometric dimensions of the plexiglass plates are 300mm×300mm×4mm, with different holes for the supporting rods and additional steel plates, and in future work NITI wires. The supporting rods are positioned to 40mm of the plexiglass plates edges, and not less, to ensure that during the vibrations the plexiglass will not break. The geometric dimensions of the supporting hollow brass rods are the exterior diameter of 4mm and the inner diameter of 3.2mm. The total length of the rods is 1m, the purchased length, and kept so, for subsequent experiments, that will support additional plates of plexiglass. To ensure that the supporting rods will not collapse during the vibrations, as well as a precision mounting of the

plexiglass plates, stiffener assemblies (fig. 9) made up of washers and nuts were used to attach the plexiglass plates to supporting rods.

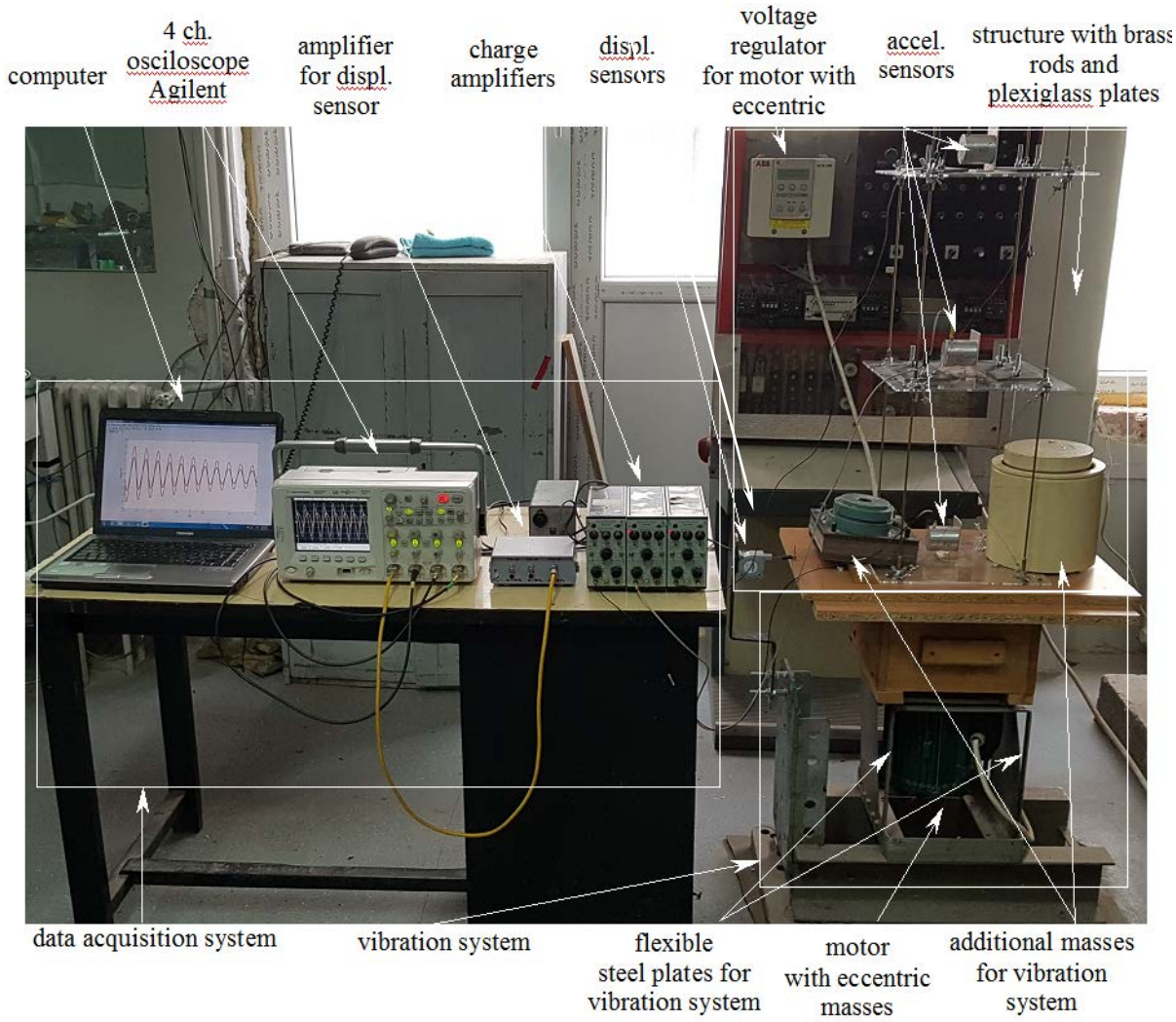

Fig.1 Experimental setup.

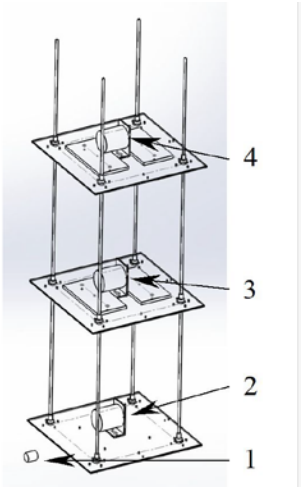

Fig. 2. Configuration 1 of sensor locations connected to 1,2,3,4 channels of the oscilloscope.

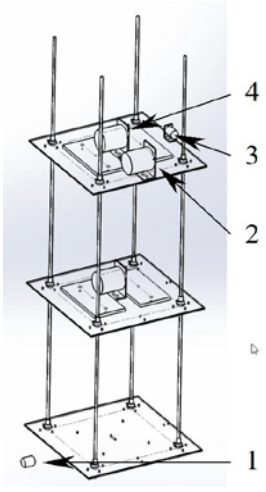

Fig. 3. Configuration 2 of sensor locations connected to 1,2,3,4 channels of the oscilloscope.

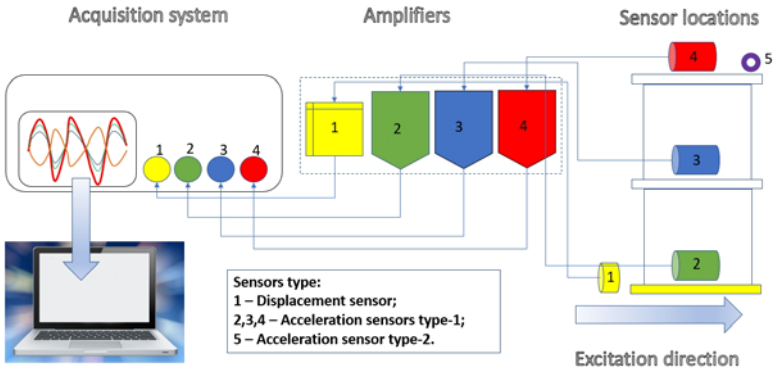

Fig. 4. Schematic diagram of the experimental data acquisition system with sensors.

Fig. 5. Bruel&Kaer Charge Amplifiers Type 2635.

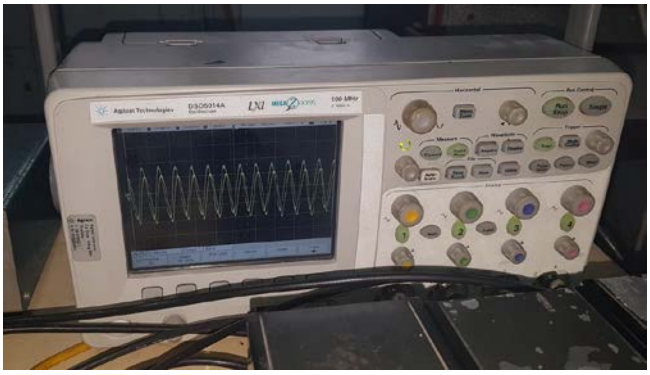

Fig.6. Acquisition system oscilloscope Agilent 5014A.

(a)

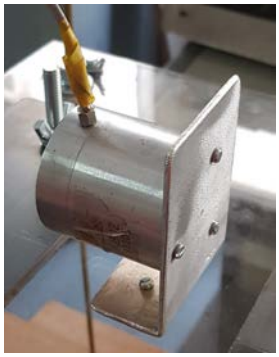

(b)

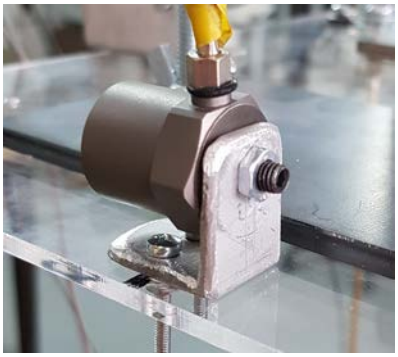

(c)

Fig.7. (a) displacement sensor, (b) accelerometer Type1 (c) accelerometer Type 2.

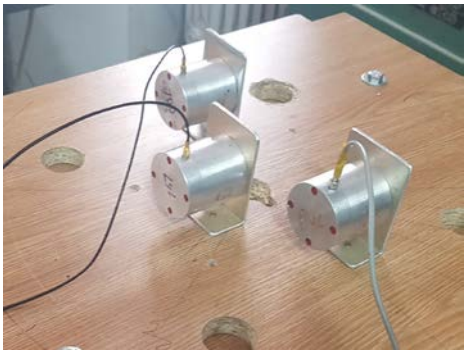

Fig. 8. Calibration of Type1 accelerometers.

Fig. 9. Stiffener with washers and nuts.

Fig.10. Vibration system.

The vibration system (Fig. 1 and Fig.10) consists of a wooden table, with additional masses, mounted on parallel very flexible steel plates, that support large deflections, to ensure minimal structural losses in the vibration system, that would be important otherwise, due to friction, in the case of a sliding system. The wooden table is excited by an electric motor with eccentric masses attached, controlled by an ABB ACS-300 AC drives for speed control. The vibrations frequencies are controlled both by the rotational speed of the electric motor and the eccentric masses attached to it.

The displacements measuring system (Fig.1, Fig. 4) consists of displacements and acceleration sensors, amplifiers with integration facilities, and an oscilloscope connected to a computer for data acquisition. One displacement sensor of type Celesco SP2-4 was used as a permanent reference of the displacements measured on the base of the structure and connected to the vibration system. Other 4 acceleration sensors, named usually accelerometers, were used to measure the displacements in various points of the vibrating structure by integration of the accelerations with amplifiers having integration facilities. Of the 4 accelerometers, one is of type Bruel&Kaer Charge Accelerometer 4381, and named by us Type2 along this paper, and the others 3 are of type HMF KB12, and named by us Type1. The 3 amplifiers with integration facilities are Bruel&Kaer Charge Amplifier type 2635. The oscilloscope used was an Agilent DSO5014A, with 4 channels, 300MHz bandwidth on 16 bits. The first channel was used to connect to the displacement sensor and used as a reference signal for the others. For the remaining 3 channels, only 3 of the 4 accelerometers were used at one time, for both configurations of sensor locations (Fig.2, Fig.3).

Experimental test planning was prepared to keep the next steps:

1) Experimental testing for calibration of the complete measurement system;
2) Experimental evaluation of the structural damping and free vibrations resonance frequency;
3) Experimental determination of the resonance frequencies for the 3 eigen modes of vibration, as well as the resonance plots.

In the first step, an experimental calibration of the complete measurement system, was done. It consists in calibration of the amplifier settings according to each sensor used, by mounting all the 3 accelerometers on the base of the vibration table (Fig. 8) and comparing with the signal given by the reference displacement sensor, at various vibration frequencies of the structure.

In the second step, an experimental determination of the structural damping was performed by a free vibration test and the measurement of the variation of the measured displacements over time at level 1 and level 2 of the structure, revealing so the exponential decrease of the amplitude vibrations as well as the resonance frequency of the structure (Fig.11). This experimental evaluation of the structural damping ratio is an essential parameter for FEM computations. In our case it was determined that the damping ratio is 1.3226%, and the resonance frequency is 2.2263 Hz, that will be confirmed in the forced vibration measurements.

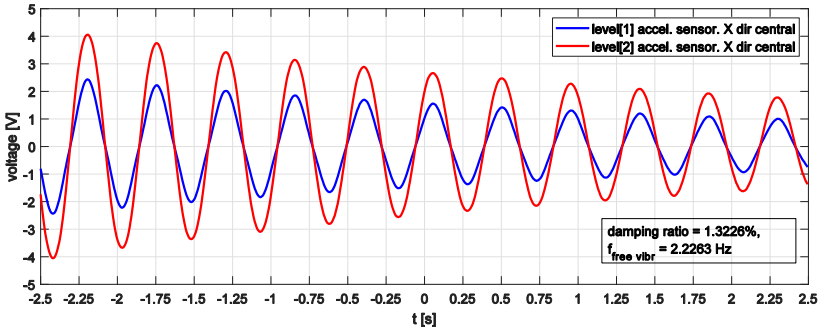

Fig. 11. Measured signal during the experimental evaluation of the structural damping.

In the third step, the most important, the resonance frequencies for the 3 vibration modes was determined. It was done by sweeping the vibration frequency from 1.25 Hz to 8.13 Hz, and recording the amplitude of displacements given by the sensors positioned in different points of the structure.

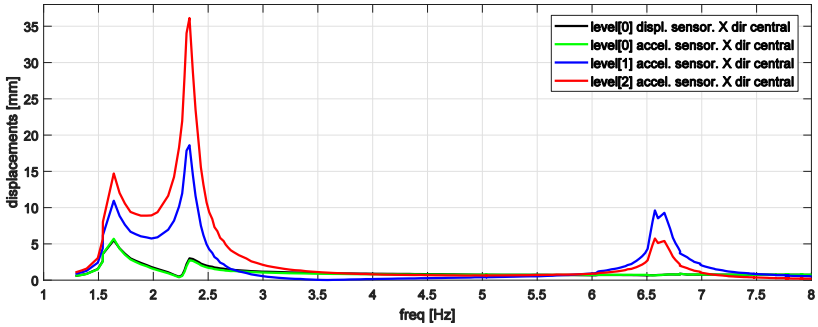

Fig. 12. Measured displacement in configuration 1 of sensor locations.

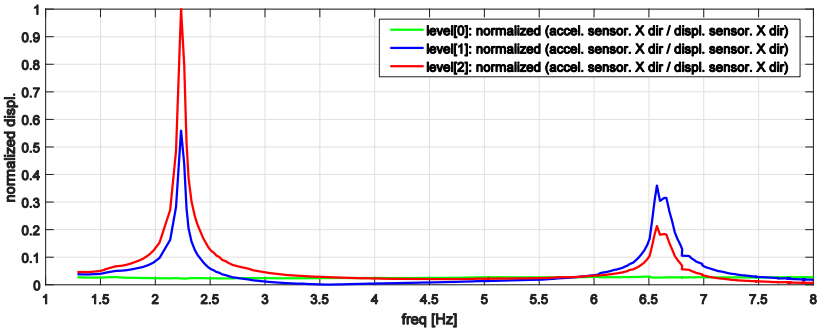

Fig. 13. Measured normalized displacement in configuration 1 of sensor locations.

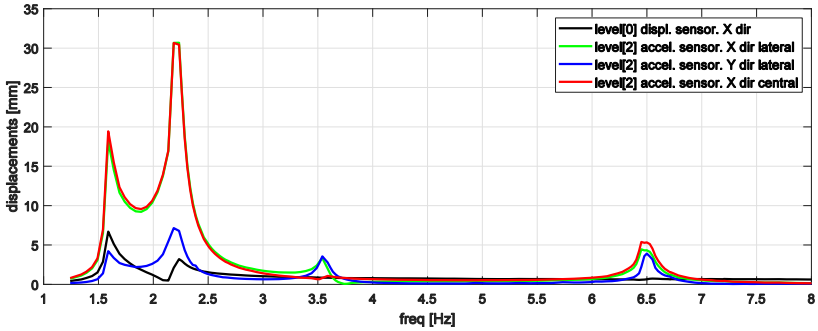

Fig. 14. Measured displacement in configuration 2 of sensor locations.

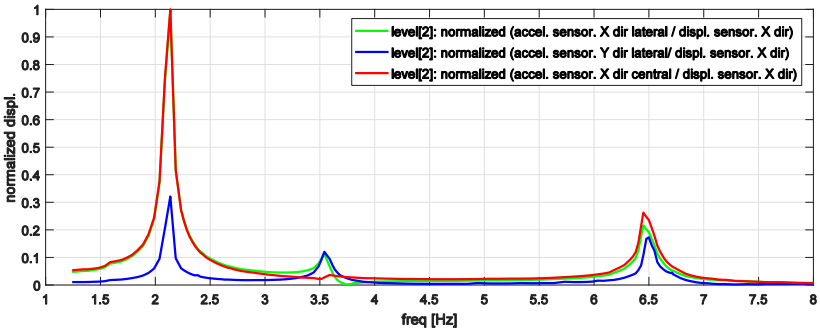

Fig. 15. Measured normalized displacement in configuration 2 of sensor locations.

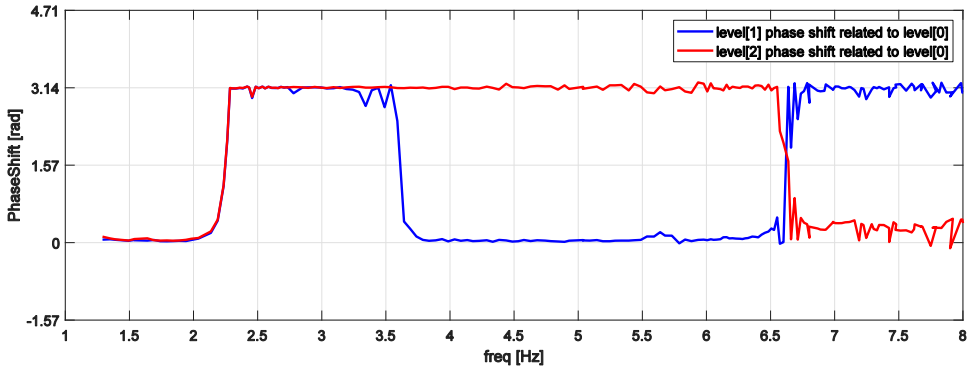

Fig. 16. Measured phase shift in configuration 1 of sensor locations.

Two sets of measurements of two different configurations (Fig. 2, Fig. 3) of accelerometer positions were considered. In both configurations the structure presents, in the range of 1.25Hz-8.13Hz) 3 eigen vibration modes, 2 for bending modes and 1 for torsion mode. These modes are shown more clearly in fig. 16 and fig. 17 in the numerical simulation section, that will confirm that the experimental results.

The first configuration of sensors position (Fig. 2) is chosen to ensure that a the resonance frequencies for the bending modes (mode 1 and mode 3, as more clearly shown in Fig. 16.b, c and Fig. 17.b,c in numerical simulation section) of the structure are revealed. As the sensors are uniaxial (measure displacements in one direction), all 3 sensors are positioned in the excitation direction (X direction) one at each level of the structure, in the center point, in order to have a symmetrical structure. The measured resonance frequency plots are presented in Fig. 12. It can be seen that the measured displacements of the vibration table are not constant, so a normalization is needed to get the correct resonance plots. They are presented in fig. 13. It can be seen that the first peak of resonance in the normalized plot is the same as the one corresponding to free vibrations (Fig.11), that proves that the normalization process is needed.

A second configuration of sensors positions (Fig.3) is chosen to ensure that the torsion mode (mode 2, as more clearly shown in Fig 16.c and 17.c in numerical simulation section) of the structure, not measured in the first configuration, is revealed. All 3 sensors are mounted on the top level of the structure, in the center on the excitation direction, and close to the edge of the structure, in both the excitation direction and perpendicular to it. The fourth sensor at the middle of the level 1 plate is not connected and it is kept as additional mass, to make the measurements as similar as possible with the ones in configuration 1. This asymmetry of the structure as well as the additional masses added to the level 2 of the structure, lead to slightly different resonance frequencies of the structure for bending modes, the ones measured for in the first configuration. The measured resonance frequency plots are presented in Fig. 14. As in the first configuration a normalization is needed to get the correct resonance plots. They are presented in Fig. 15. It can be seen that, around the first bending mode sensors 2 and 4 recorded the same values, and around the torsion mode sensors 2 and 3 recorded the same values. That proves that the sensors were well calibrated.

From Fig. 12 and Fig. 14 it can be seen that the complete FRF investigation reveal also a vibration-absorber behavior of the structure against vibration system assembly, with resonance peak before the first bending mode.

As the excitation frequency increases a phase shift is present between the signals measured at the level 1 and level 2 of the structure related to the signal measured at level 0. It is plotted in Fig. 16.

1. NUMERICAL FEM RESULTS. COMPARISON WITH EXPERIMENTAL ONES

The FEM computations were done in Comsol 5.3, in both eigenfrequency and frequency domain study, for both configurations of the sensors, with a slightly simplified geometric model (Fig 17. a and 18.a), to shorten the computational time and resources needed.

The stiffener assemblies made up of washers and nuts in experiments (Fig. 9) were simplified to steel cylinders surrounding the rods around the joints with plexiglass plates. For these simplified stiffeners the geometric dimensions taken in simulations are: outer diameter of 8mm, inner diameter of 4mm and length of 50mm. The Type1 and Type2 sensors were approximated to blocks of aluminum and steel with the same weight as the real ones of 225g, and 55g respectively. The elastic properties of the brass rods were approximated to copper rods. The additional steel plates are considered bonded, and not attached with screws.

The parameters for grid size were taken 'finer' for the brass hollow rods (approximated to copper hollow rods) and steel stiffeners, and only 'fine' for plexiglass plates, steel plates and simplified aluminum 2024 and steel sensors blocks. Additional parameters are the fixed constraints (0 displacements) considered for the bottom side of the level 0 plexiglass plate, for both eigenfrequency and frequency domain study. The structural losses have been considered of 1.3%, as in the experimental determination of it at the resonance frequency, even it is known that it is not constant for all frequencies, in fact increasing with frequency.

The elastic properties of the materials, modulus of elasticity E , Poisson ratio ν, mass density ρ, taken in the FEM simulations are taken mainly from the Comsol 5.3 library, and are

- for copper: $E = 126\ GPa$, $\nu = 0.335$, $\rho = 8940\ kg/m^3$
- for plexiglass: $E = 3.0\ GPa$, $\nu = 0.4$, $\rho = 1190\ kg/m^3$
- for steel: $E = 211.9\ GPa$, $\nu = 0.228$, $\rho = 7860\ kg/m^3$
- for aluminum 2024: $E = 73.14\ GPa$, $\nu = 0.331$, $\rho = 2780\ kg/m^3$

TABLE 1. Resonance frequencies measured experimentally and computed with FEM.

Eigen mode	Experimental results		Numerical FEM results	
	sensor config 1	sensor config 2	sensor config 1	sensor config 2
	Freq [Hz]	Freq [Hz]	Freq [Hz]	Freq [Hz]
1 bending	2.234	2.13	2.34	2.04
2 torsion	---	3.54	4.17	3.62
3 bending	6.68	6.48	6.62	6.48

The FEM eigenfrequency study shows the presence of 3 vibrations mode, mode 1 and mode 3 for bending modes (Fig.17.a, c and Fig.18.a, c) and mode 2 for torsion mode (Fig.17.b and Fig.18.b). They are computed for both configurations, and can be seen as peaks in fig. 19 and fig. 20, in normalized displacements plots. For a better comparison of the experimental and numerical values for the 3 vibration modes, table 1 has been done. It can be seen that the differences between the values measured experimentally and computed numerically are less than 5%, bellow the 10% accepted usually in numerical-experimental comparisons. From Fig. 17 and Fig. 18, but also from table 1, it can be seen that the asymmetric sensor position of the Type1 sensor at the edge of the plate, alters the resonance frequency for both bending modes as well as for torsion modes.

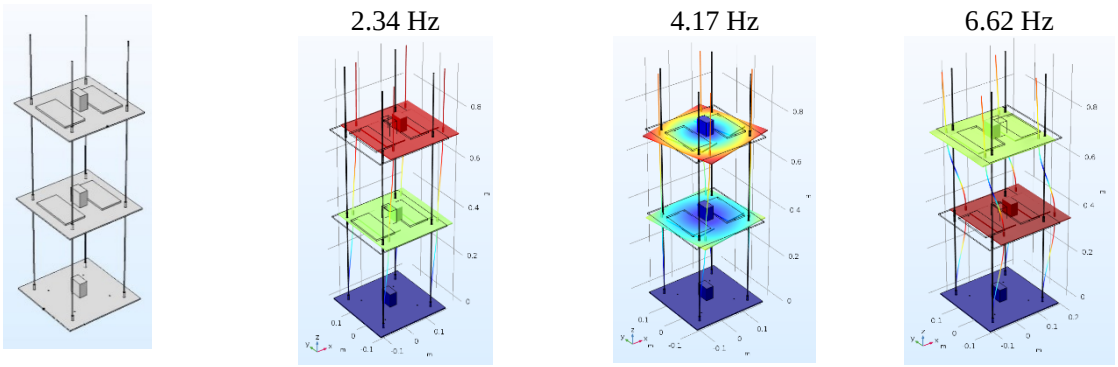

Fig. 17. (a) Simplified geometry taken in FEM computation, (b), (c), (d) computed FEM mode shapes for structure in configuration 1 of sensors locations.

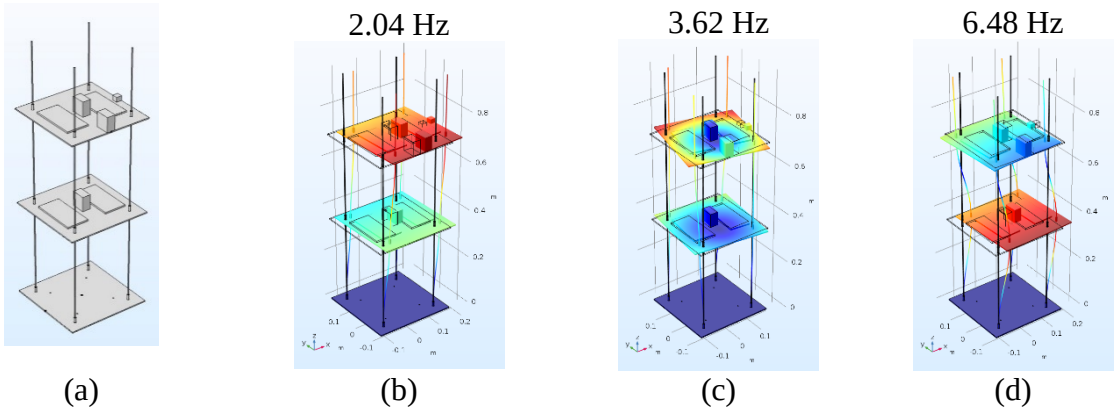

Fig. 18. (a) Simplified geometry taken in FEM computation, (b), (c), (d) computed FEM mode shapes for structure in configuration 2 of sensors locations.

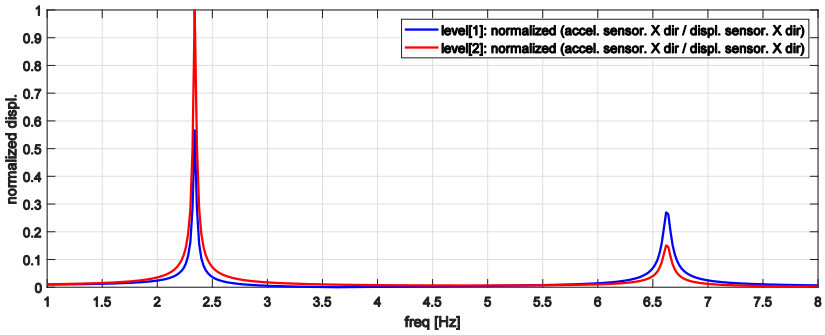

Fig. 19. Computed FEM normalized displacement in configuration 1 of sensor locations.

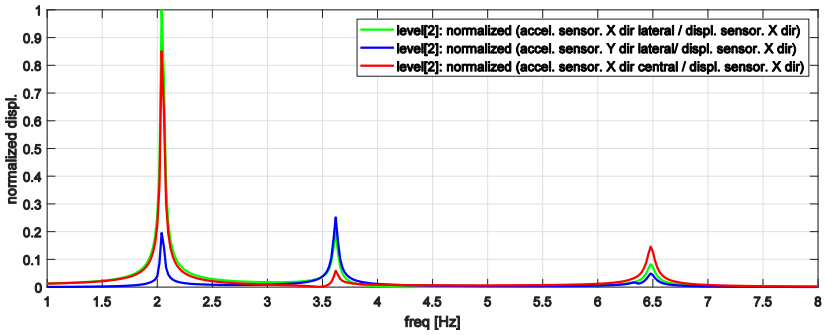

Fig. 20. Computed FEM normalized displacement in configuration 2 of sensor locations.

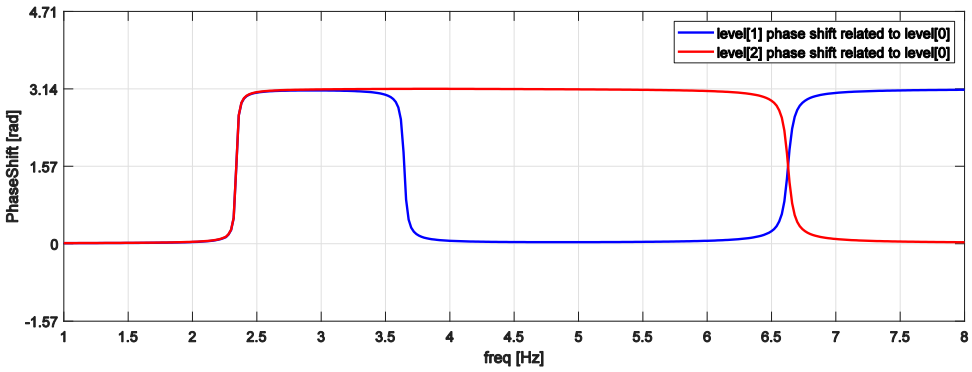

Fig. 21. Computed phase shift in configuration 1 of sensor locations.

The FEM frequency study was done for o comparison of the experimental plots from Fig. 12-fig.15 with the numerical ones. The computed frequency domain was 1.0 Hz - 8.0 Hz in steps of 0.02 Hz. The point where the values were computed are the center and middle edges of the plexiglass plates at the upper surfaces, in close proximity of the sensor's locations. The computed plots in normalized values are presented in fig. 19 for sensor configuration 1, and in fig. 20 for sensor configuration 2. The plots presents the computed modulus of displacement in the sensing direction of the accelerometers: Ox for Type1 and Oy for Type2: $\sqrt{\mathrm{Re}(u)^2+\mathrm{Im}(u)^2}$ and respectively $\sqrt{\mathrm{Re}(v)^2+\mathrm{Im}(v)^2}$, were u and v are the computed displacements in the Ox and Oy directions, both complex values. I can be seen that the computed FEM plots (fig. 19 and fig. 20) agree well with the measured experimental plots (Fig. 13 and Fig. 15).

A computed phase shift of computed displacements of the signals measured at the level 1 and level 2 of the structure related to the signal measured at level 0, is plotted in fig. 21. By a visual comparison of the computed (fig. 21) and measured (fig. 16) phase shift, it can be seen that as the frequency increases, the differences between measured and computed values also increases, with maximal differences around the third vibration mode (bending), but overall the trend is kept.

2. CONCLUSIONS

This paper is the first part of a study concerning the vibration of a structure made of 2 level frames, that includes NiTi wires as passive and active dampers.

This first part presents the experimental setup, the experimental measurements and numerical FEM computation, of the vibrations of structure *without* NiTi wires, as a starting point for a future study.

The experimental setup was shown to be suited to measure the resonance frequencies of the 2-level structure, in the vibration excitation direction. The geometrical dimensions of the structure with hollow brass rods and plexiglass plates, and stiffener assemblies at the joints between brass rods were well chosen to support large deflection vibrations, compared to its size, as well as stiff enough to not collapse at resonance frequencies. A good vibration system controlled in frequency was used. A sensitive displacement measuring acquisition system ensured a good quality of the measurements, and so a meaningful comparison with numerical results.

Experimental investigation reveals also a vibration-absorber behavior of the structure against vibration system assembly. The displacements amplitude of the vibration table was not constant. So, a normalization of the measured displacement was needed, and used successfully.

The results of this experimental modal analysis were compared with numerical FEM computation, both in eigenfrequency and in domain frequency studies, and good agreement was found. Differences between measured and computed values of 5% and less, are bellow the 10% accepted in experimental-computed comparisons.

The simplifying assumptions in the geometric model taken in FEM computations as well as approximated material properties and grid size, were well chosen to ensure both enough accuracy as well as good computation speed.

Further investigations will include resonance frequencies of the 2 level frame structure, considered in this study, but in the *presence* of NiTi wires; Investigation of the changes of the resonance frequencies related to the tension in NiTi wires, in this studied structure; Analytical, numerical and experimental investigation of active vibration control system using memory-alloy materials into structure, should also be included.

Acknowledgements. The authors thanks to Dr. Tudor Sireteanu, Dr. Veturia Chiroiu and Dr. Ligia Munteanu for fruitful discussions and meaningful suggestions.

REFERENCES

1. ANDRAWES, B., MCCORMICK, J., DESROCHES, R., *Effect of cycling modeling parameters on the behavior of shape memory alloys for seismic applications*, SPIE Conference on Smart Structures and Materials, 2004.
2. AURICCHIO, F., SACCO, E.,*Thermo-mechanical modelling of a superelastic shape- memory wire under cyclic stretching-bending loadings*, International Journal of Solids and Structures, Vol. 38, pp. 6123–6145, 2001.
3. CORBI, O., *Shape memory alloys and their application in structural oscillations attenuation*, Simulation Modelling Practice and Theory, Vol. 11, pp. 387–402, 2003.
4. FUGAZZA, D., *Shape-memory alloy devices in earthquake engineering: mechanical properties, constitutive modelling and numerical simulations*, Master's thesis, European School of Advanced Studies in Reduction of Seismic Risk (ROSE School) 2003.
5. MISHRA J., *Smart materials-types and their application: A Review*, International Journal of Mechanical And Production Engineering, 5(12), 2320–2322, 2017.
6. MOHD J, LEARY M, SUBIC A, et al., *A review of shape memory alloy research, applications and opportunities*, Mater. Des., 56,1078–1113, 2014.
7. TOBUSHI, H., SHIMENO, Y., HACHISUKA, T., TANAKA, K., *Influence of strain rate on superelastic properties of TiNi shape memory alloy*, Mechanics of Materials, Vol. 30, pp. 141–150, 1998.
8. STRNADEL, B., OHASHI, S., OHTSUKA, H., ISHIHARA, T., MIYAZAKI, S., *Cyclic stress-strain characteristics of Ti-Ni and Ti-Ni-Cu shape memory alloys*, Materials Science and Engineering, Vol. 202, pp. 148–156, 1995.
9. TAMAI, H., KITAGAWA, Y., *Pseudoelastic behavior of shape memory alloy wire and its application to seismic resistance member for building*, Computational Materials Science, Vol. 25, pp. 218–227, 2002.
10. SADAT, S., SALICHS, J., NOORI, M., HOU, Z., DAVOODI, H., BAR-ON, I., SUZUKI, Y., MASUDA, A., *An overview of vibration and seismic applications of NiTi shape memory alloy, Smart Materials and Structures*, Vol. 11, pp. 218–229, 2002.
11. BARZEGARI, M.M., DARDEL, M., FATHI, A., *Vibration analysis of a beam with embedded shape memory alloy wires*, Acta Mech. Solida Sin., 26, 536–550, 2013.
12. MORE, D.J., CHAVAN, S.A., *Frequency Response of Sandwich Beam Embedded With Shape Memory Alloy Wires*, Procedia Mater. Sci., 10, 638–643, 2015.
13. SONG, G., KELLY, B., AGRAWAL, B.N., *Active position control of a shape memory alloy wire actuated composite beam*, Smart Mater. Struct, 9, 711-716, 2000.
14. NOOLVI, B., RAJA, S., NAGARAJ, S., et al., *Fabrication and testing of SMA composite beam with shape control*, AIP Conference Proceedings 1859, paper 020055, 2017.
15. WILSON, J., WESOLOWSKY, M., *Shape memory alloys for seismic response modification: a state-of-the-art review*, Earthquake Spectra, Vol. 21, pp. 569–601, 2005.
16. WILDE, K., GARDONI, P., FUJINO, Y., *Base isolation system with shape memory alloy device for elevated highway bridges*, Engineering Structures, Vol. 22, pp. 222– 229, 2000.
17. CROCI, G., BONCI, A., VISKOVIC, A., *Use of shape memory alloy devices in the basilica of St Francis of Assisi*, Proceedings of the Final Workshop of ISTECH Project - Shape Memory Alloy Devices for Seismic Protection of Cultural Heritage Structures, pp. 110–133, 2000.

18. MAZZOLANI, F. M., MANDARA, A., *Modern trends in the use of special metals for the improvement of historical and monumental structures*, Engineering Structures, Vol. 24, pp. 843–856, 2002.
19. INDIRLI, M., *The demo-intervention of the ISTECH Project: the bell tower of S. Giorgio in Trignano (Italy)*, Proceedings of the Final Workshop of ISTECH Project - Shape Memory Alloy Devices for Seismic Protection of Cultural Heritage Structures, pp. 134–146, 2000.
20. INDIRLI, M., CARPANI, B., MARTELLI, A., CASTELLANO, M. G., INFANTI, S., CROCI, G., BIRITOGNOLO, M., BONCI, A., VISKOVIC, A., VIANI, S., *Experimental tests on masonry structures provided with shape memory alloy antiseismic devices*, 12th World Conference in Earthquake Engineering, pp. 1–8, 2000.
21. FUGAZZA, D., *Shape-memory alloy devices in earthquake engineering: mechanical properties, constitutive modelling and numerical simulations*, Master's thesis, European School of Advanced Studies in Reduction of Seismic Risk (ROSE School), 2003.
22. MIHAILESCU, M., CHIROIU, V., *Advanced mechanics on shells and intelligent structures*, Publishing House of the Romanian Academy, 2004.
23. CHIROIU, V., IONESCU, M.F., SIRETEANU, T., IOAN, R., MUNTEANU, L., *On intrinsic time measure in the modeling of cyclic behavior of a Nitinol cubic block*, Smart Materials and Structures, 24(3), 035022 1-11, 2015.
24. CHIROIU, V., MUNTEANU, L., *A flexible beam actuated by a shape memory alloy ribbon*, Proceedings of the Romanian Academy, Series A: Mathematics, Physics, Technical Sciences, Information Science, 4(1), 45–51, 2003.
25. BROCCA, M., BRINSON, L.C., BAZZANT, Z.P., *Three- dimensional constitutive model for shape memory alloys based on microplane model*, Journal of the Mechanics and Physics of Solids 50, p.1051 – 1077, 2002.

Received March 10, 2019